J Mol Model (2013) 19:1143–1151
DOI 10.1007/s00894-012-1662-2

ORIGINAL PAPER

Theoretical study on the encapsulation of Pd_3-based transition metal clusters inside boron nitride nanotubes

Qing Wang · Yue-jie Liu · Jing-xiang Zhao

Received: 30 August 2012 / Accepted: 22 October 2012 / Published online: 13 November 2012

Abstract Chemical functionalization of the boron nitride nanotube (BNNT) allows a wider flexibility in engineering its electronic and magnetic properties as well as chemical reactivity, thus making it have potential applications in many fields. In the present work, the encapsulation of 13 different Pd_3M (*M*=Sc, Ti, V, Cr, Mn, Fe, Co, Ni, Cu, Zn, Pd, Pt, and Au) clusters inside the (10, 0) BNNT has been studied by performing comprehensive density functional theory (DFT) calculations. Particular attention is paid to searching for the stable configurations, calculating the corresponding binding energies, and evaluating the effects of the encapsulation of Pd_3M cluster on the electronic and magnetic properties of BNNT. The results indicate that all the studied Pd_3M clusters can be stably encapsulated inside the (10, 0) BNNT, with binding energies ranging from −0.96 (for Pd_3Sc) to −5.31 eV (for Pd_3V). Moreover, due to a certain amount of charge transfer from Pd_3M clusters to BNNT, certain impurity states are induced within the band gap of pristine BNNT, leading to the reduction of the band gap in various ways. Most Pd_3M@BNNT nanocomposites exhibit nonzero magnetic moments, which mainly originate from the contribution of the Pd_3M clusters. In particular, the adsorption of O_2 molecule on BNNT is greatly enhanced due to Pd_3M encapsulation. The elongation of O-O bonds of the adsorbed O_2 molecules indicates that Pd_3M@BNNT could be used to fabricate the oxidative catalysis.

Q. Wang · Y.-j. Liu · J.-x. Zhao (✉)
Key Laboratory for Photoelectric Bandgap Materials, Ministry of Education, School of Chemistry and Chemical Engineering, Harbin, Harbin Normal University, Harbin 150025, China
e-mail: xjz_hmily@yahoo.com.cn

Q. Wang
College of Chemistry, Beijing Normal University, Beijing 100875, China

Keywords Boron nitride nanotube · DFT · Encapsulation · Pd_3M cluster

Introduction

Since its discovery in 1991 [1], the carbon nanotube (CNT) has attracted increasing attention due to its potential applications. The impressive progress in CNT research has motivated scientists to explore other 1D atomic based materials. Among them, the boron nitride nanotube (BNNT) [2] has become a hotly pursued system, as it shares the same honeycomb lattice structure as CNT. Although BNNT has similar geometry as CNT, it may have more important advantages over CNT. For example, BNNTs not only have high thermal conductivity but also high oxidation resistivity as well as high thermal and chemical stability [3, 4]. These properties render them good candidates for developing nanotube-based devices in hazardous and high-temperature environments.

Moreover, BNNTs are semiconductors with a wide band gap (~5.5 eV) that are weakly dependent on the tube diameter, chirality, and the number of walls [5–7]. The poor electrical conductivity has imposed great limitations for electronic application of BNNTs. To overcome this obstacle, the most popular method is to modify its electronic properties and to enhance its solubility by chemical functionalization. Many significant efforts have been made for this issue [3, 8–12]. For example, Xie and co-workers have experimentally obtained a soluble BNNT via functionalization with amino-based compounds [8]. Zhi et al. have connected a long alkyl chain to a BNNT via a successful chemical reaction, making the functionalized tubes be soluble in many solvents [11]. Theoretically [13–31], H [13–16], F [17–22], metal [23], NH_3 [24, 25], CCl_2 molecules [26–28], and noncovalent functionalization with organic

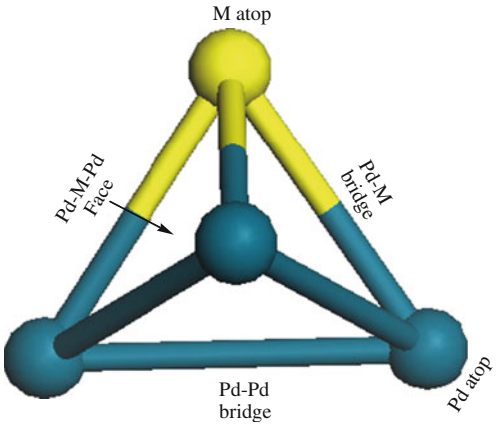

Fig. 1 Various adsorption sites considered for Pd_3M cluster encapsulation inside the (10, 0) BNNT

molecules [31, 32] have been shown to modify the properties of BNNTs. These studies on the chemical functionalization of BNNTs are important to provide a guidance to design BNNTs-based devices.

In particular, BNNTs filling with molecules/clusters and continuous nanowires made of metals or inorganic compounds may become an interesting and practically important field. This is because the BNNTs are especially suitable for the task of shielding the metallic nanowires inside their cavity to protect the encapsulated content from oxidation during fabrication and application. More importantly, the presence of impurity metal atoms and clusters inside BNNTs during their synthesis can significantly modify the physicochemical properties and that can differ considerably on the geometry and confinement of the host material. To understand this effect of confinement many experimental and theoretical studies have reported on metal encapsulated BN nanomaterials [33–41]. Zhi and co-workers have summarized filled various materials in BNNTs, including metals and semiconductors [4]. These filled BNNTs can be rather useful. For example, metal-filled BNNTs can be nanoscale "lacquered" wire [33] or natural "pipelines" for delivery of tiny metallic clusters under applied thermal, magnetic, or electric fields [34]. C_{60}-filled BNNTs can work as a special nanoswitch [33]. The interesting electron field-emission of SiC-filled BNNTs can be found [35] and MgO_2-filled BNNTs can be used as oxygen generator [36]. Theoretically, the effects of the encapsulation of Fe, Co, Ni, and Cu nanowires on the properties of BNNTs have been reported [37–44]. For example, Xiang et al. have shown that the Ni encapsulated (9, 0) BNNT exhibits interesting semi-half-metallic behavior [37], while Ghosh and co-workers have underscored the possibility of functionalizing these encapsulated BNNTs by interacting them with oxygen molecules [44].

Compared with these above studies, we note that the theoretical reports on the alloys filling in BNNTs are considerable lacking, which is very important not only for deeply understanding the properties of BNNTs, but also for further widening the application fields of BNNTs. Here, using density functional theory (DFT), we have explored the encapsulation of a series of Pd_3M alloys inside a (10, 0) BNNT as an example, where M is Sc, Ti, V, Cr, Mn, Fe, Co, Ni, Cu, Zn, Pt, Pd, or Au, respectively. In particular, the following questions would be mainly addressed: (1) can these Pd_3M stably exist inside the (10, 0) BNNT? (2) If yes, how do the electronic properties of (10, 0) BNNT modify? (3) Whether these Pd_3M clusters can retain their magnetic properties inside BNNT? Apart from these fundamental aspects, one of the primary objectives of this study is to investigate the chemical reactivity of these filled BNNTs by Pd_3M toward oxygen molecule.

Theoretical methods and models

In the present work, we used DFT methods, implemented in the Dmol^3 package [45, 46], to study the encapsulation of Pd_3M cluster inside the BNNT. All-electrons calculations

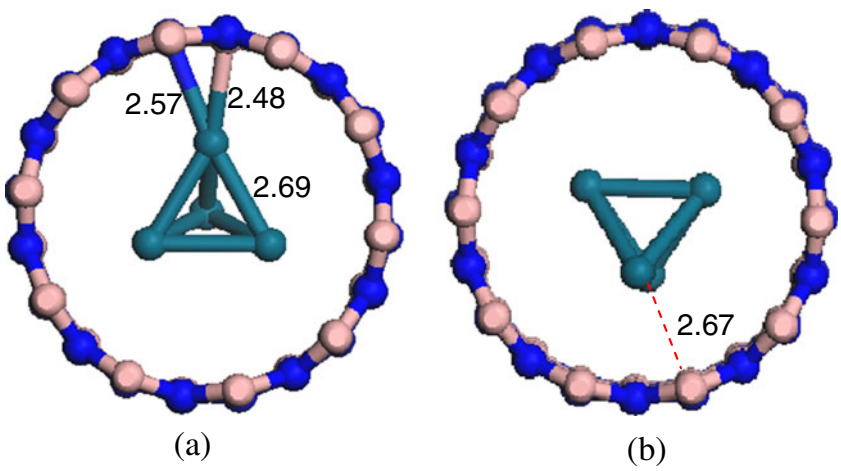

Fig. 2 The obtained stable configurations of Pd_4 cluster encapsulated inside the (10, 0) BNNT: **a** Config_1 and **b** Config_2. The unit of bond length is Å

were employed with the double numerical basis sets plus polarization functional (DNP). The generalized-gradient approximation (GGA) with the Perdew-Burke-Ernzerhof (PBE) [47] and the local density approximation (LDA) with the Perdew-Wang (PWC) functional [48] were applied to estimate a range of the binding energy. In fact, LDA has been shown to be a reliable functional to study the systems involving the van der Waals interactions [49–51] and can give an adsorption energy much closer to the MP2 calculation [52–54]. Additionally, the PBE/DNP method has also been used widely in the study of weak interactions [55–58]. In the present work, GGA with the PBE method is utilized as the exchange-correlation functional throughout the paper. For the 5*d* transition metal atoms Pd, Pt, and Au, the scalar relativistic effect (DSSP) was considered when dealing with their core electrons. The Hirshfeld population analysis [59] was used to obtain both the charges and the net spin populations on each atom. Spin-unrestricted DFT calculations were carried out for Pd_3M cluster filled in the (10, 0) BNNT with a diameter of 7.94 Å in a periodically repeating tetragonal super cell, whose lattice constants is $a=b=20$ Å and c (c is taken to be twice the one-dimensional lattice parameter of the pure BNNT). The Brillouin zone of the super cell is sampled by $1\times1\times3k$ points within the Monkhorst-pack scheme [60]. It should be mentioned that we do not consider the encapsulation of Pd_3M cluster inside other BNNTs. This is because, for those BNNTs with larger diameters, the encapsulated molecules move almost freely along the nanotube, and eventually leave it. On the contrary, due to being compressed inside BNNTs with smaller diameters, the filled molecules may be excessively compressed, leading to a large structural change for these filled clusters. Thus, they may not stably exist.

Results and discussion

To determine the stability of the encapsulated Pd_3M (M=Sc, Ti, V, Cr, Mn, Fe, Co, Ni, Cu, Zn, Pd, Pt, and Au) cluster in the BNNT, we first calculated the binding energy, E_b, which is defined as the difference between the total energy of the Pd_3M clusters encapsulated in the BNNT ($E_{Pd3M@BNNT}$), and the sum of the total energies of the (10, 0) BNNT (E_{BNNT}), and the isolated Pd_3M cluster (E_{Pd3M}): $E_b = E_{Pd3M@BNNT} - E_{Pd3M} - E_{BNNT}$. For each type of the adsorbate, five different configurations were selected to examine the Pd_3M encapsulation into (10, 0) BNNT, i.e., (1) Pd atop, (2) M atop, (3) Pd–M bridge, (4) Pd–Pd bridge, and (5) Pd–M–Pd face, as shown in Fig. 1, are attached to the inner wall of (10, 0) BNNT, respectively.

Using the Pd_4 case as an example (Fig. 2), for which two stable configurations are obtained: (1) Pd_4 cluster is attached to one side of (10, 0) BNNT, as shown in Fig. 2a (labeled as Config–1). (2) The Pd_4 cluster is locating at the center of the (10, 0) BNNT (Fig. 2b, Config–2). In the former configuration, the shortest B–Pd and N–Pd bond lengths are 2.48 and 2.57 Å, respectively. For the Config–2, one Pd–Pd bond is parallel to the tube axis, while the other one is perpendicular to the tube axis. The nearest distance between Pd_4 cluster and BNNT is about 2.67 Å. Moreover, the symmetry of the Pd_4 clusters in the above two structures change little after being coated by (10, 0) BNNT. After being inserted, the Pd_4 cluster expands a little, e.g., the average Pd–Pd distance in a free Pd_4 cluster changes from 2.63 to 2.69 Å in Pd_4@(10, 0) BNNT, and the nanotube walls expand slightly, 0.02 Å for the (10, 0) BNNT. The calculated binding energies for Config–1 and 2 are −1.63 and −1.49 eV, respectively. The negative binding energy value indicates that the encapsulation process of Pd_4 cluster into (10, 0) BNNT is exothermic.

Among the other 12 Pd_3M clusters considered, the LDA and GGA predict that they can be stably encapsulated inside the (10, 0) BNNT. As expected, the LDA gives a slightly stronger interaction between the Pd_3M clusters and BNNT. We note that the calculated binding energies range from −0.96 (GGA) to −5.31 eV (GGA), for Pd_3Sc and Pd_3V, respectively, as shown in Table 1. The variation of the shortest distance between Pd_3M and BNNT is consistent with the binding energy, ranging from 2.41 (for Pd_3V) to 2.53 Å (for Pd_3Sc). In summary, based on the calculated binding energies, we speculate that those Pd_3M clusters can be stably filled in the (10, 0) BNNT. Correspondingly, the obtained configurations of Pd_3M@BNNTs are presented in Fig. 3.

Table 1 Calculated binding energy (E_b, eV) of a Pd_3M cluster encapsulated inside the (10, 0) BNNT, the corresponding shortest distance between Pd_3M cluster and BNNT (d, Å), the charge transfers from the Pd_3M cluster to BNNT (Q, e), and the net magnetic moments of the M atom/total system

M	E_b[a]	d	Q	μ_M/μ_{total}
Sc	−0.96 (−1.24)	2.53	0.33	0
Ti	−1.81 (−2.32)	2.44	0.39	1.44/1.84
V	−5.31 (−5.92)	2.41	0.36	2.59/2.99
Cr	−4.67 (−5.16)	2.42	0.42	3.77/4.09
Mn	−2.97 (−3.31)	2.46	0.63	5.01/5.08
Fe	−2.89 (−3.14)	2.44	0.37	3.81/3.91
Co	−1.69 (−2.20)	2.46	0.59	2.90/2.94
Ni	−1.78 (−2.04)	2.52	0.37	1.86/1.91
Cu	−1.70 (−1.97)	2.46	0.53	0.43/0.44
Zn	−1.43 (−1.75)	2.46	0.61	0
Pd	−1.63 (−1.82)	2.48	0.56	1.49/1.58
Pt	−1.82 (−2.01)	2.45	0.48	1.32/1.40
Au	−1.77 (−1.95)	2.46	0.52	0.04/0.05

[a] Values in parentheses are derived from the LDA/PWC method

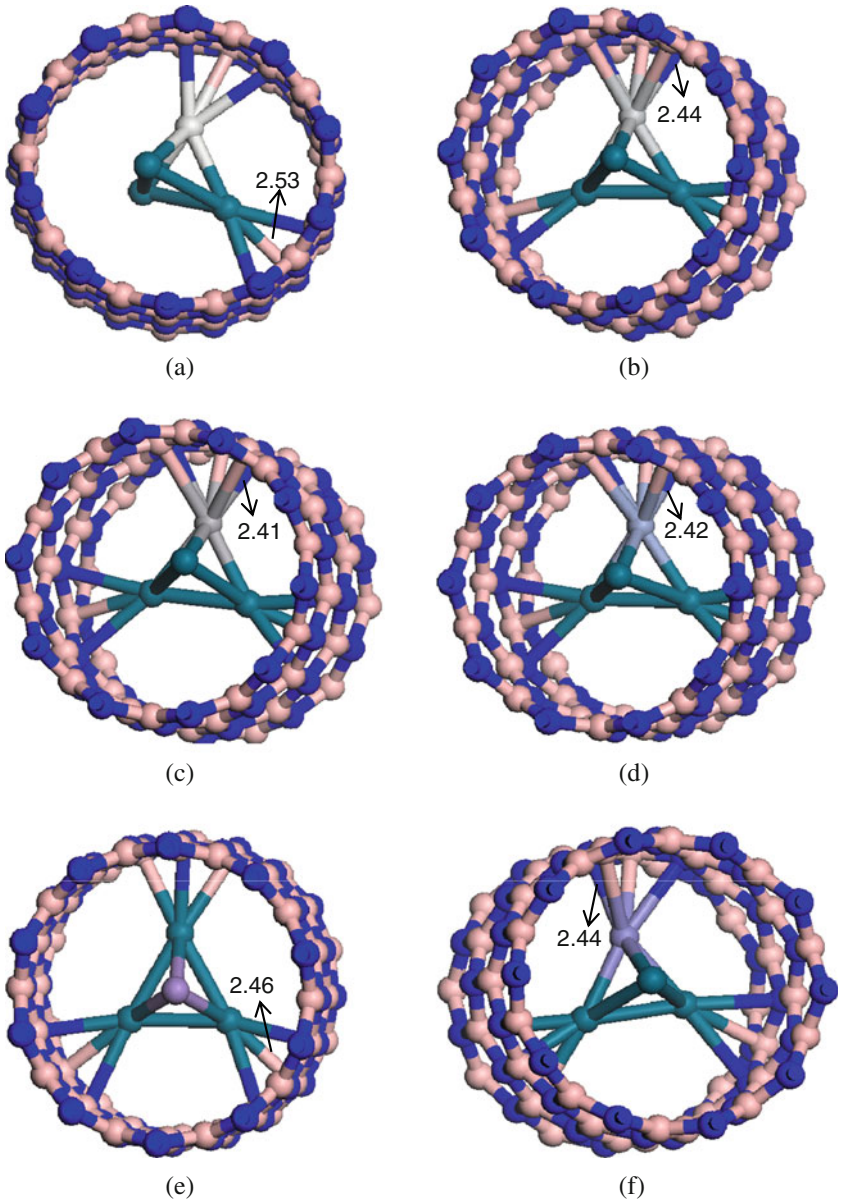

Fig. 3 The obtained most stable configurations of Pd_3M cluster encapsulated inside the (10, 0) BNNT, where M is **a** Sc, **b** Ti, **c** V, **d** Cr, **e** Mn, **f** Fe, **g** Co, **h** Ni, **i** Cu, **j** Zn, **k** Pt, and **l** Au. The unit of bond length is Å

In addition to the binding energies and local-minimum configurations, we have examined the effects of Pd_3M clusters encapsulation on the electronic structures of (10, 0) BNNT. Based on the spin unrestricted calculations, the band structures of the pristine (10, 0) BNNT as well as those of the most stable 13 Pd_3M@BNNT systems are calculated. Both the plus and minus spins (labeled with "+" and "–" in Fig. 4) were considered. For the pristine BNNT, the band structures for the plus and minus spins are the same, exhibiting a direct band gap of 4.13 eV (Fig. 5a). Moreover, it can be seen from Fig. 5 that in all 13 systems the encapsulation of the Pd_3M clusters induces certain impurity states within the band gap of the pristine BNNT, thereby leading to the band gap reduction. In most cases, the band gap is no greater than 1.0 eV. The results of projected density of states (PDOS) indicate that these impurity states mainly due to the *d* electrons of the Pd_3M clusters. To some extent, the *p* electrons also contribute to the density of states near the Fermi level, but the contribution is much less than the *d* electrons. The BNNT contributes little to the density of states near the Fermi level.

The electron-charge analysis using the Hirshfeld method is summarized in Table 1. With the encapsulation of Pd_3M clusters inside BNNTs, certain amount charge is transferred from Pd_3M clusters to BNNT, ranging from 0.33 *e* (Pd_3Sc) to 0.63 *e* (Pd_3Mn). As a result, a net magnetic moment may emerge. Because the ground state of the pristine BNNT is nonmagnetic, the net spin mainly origins from the magnetism of Pd_3M clusters as shown in Table 1. Moreover, Pd_3M encapsulation also leads to an induction of local magnetic moment on the N atoms. This is expected, because the 3*d* orbitals of Pd_3M clusters gets partially hybridized with N 2*p*

Fig. 3 (continued)

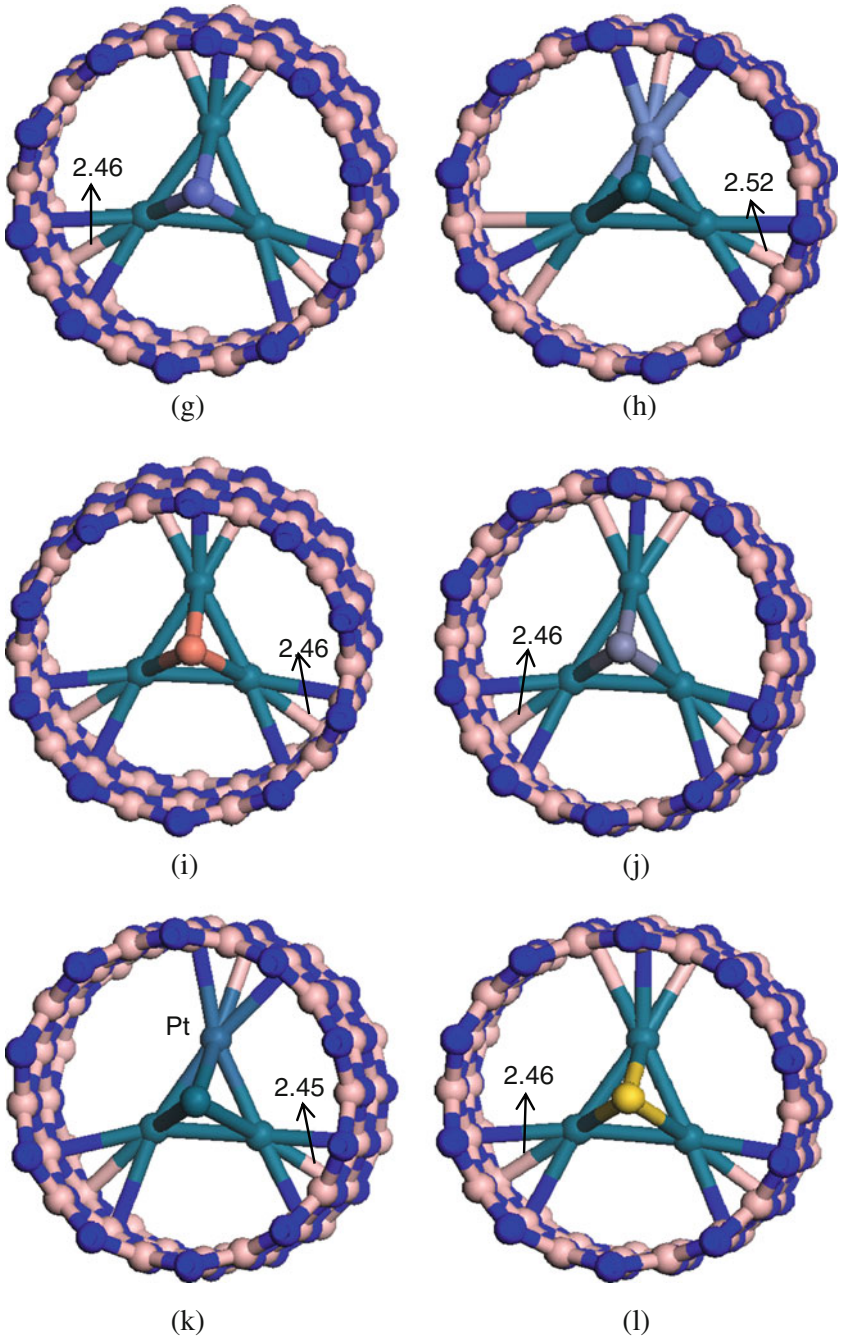

states. Among all Pd_3M clusters that have been studied here, Pd_3Mn shows the largest spin polarization (total magnetic moment of 5.08 μ_B), whereas that of Pd_3Au is smallest (total magnetic moment of 0.05 μ_B), and the value decreases to 0 for Pd_3Zn. The small magnetic moment of filled BNNT by Pd_3Zn and Pd_3Au seems to correlate with the valence shell of Zn and Au: Zn has a filled valence shell (there is no unpaired electron) and Au has only one unpaired electron in its valence shell. Thus, when the two clusters are filled inside BNNT, their valence electrons involve in interaction with BNNT, decreasing their magnetic moment, compared with their freestanding ones. In terms of the unique properties, the filled BNNT by some Pd_3M clusters (such as Pd_3Mn) may have potential applications in spintronic and quantum information.

Due to the appearance of mid-gap states around Fermi level of Pd_3M@BNNT and charge transfer between BNNT and Pd_3M clusters, the chemical reactivity of BNNT may be enhanced to different degrees. To verify this fact, we have studied the adsorption of an O_2 molecule on Pd_3M@BNNT composites and compared it with that on pristine BNNT. The calculation is performed by placing a single O_2 molecule on Pd_3M@BNNT in vertical or horizontal orientations at different sites, including atop of B or N, edge of the B–N

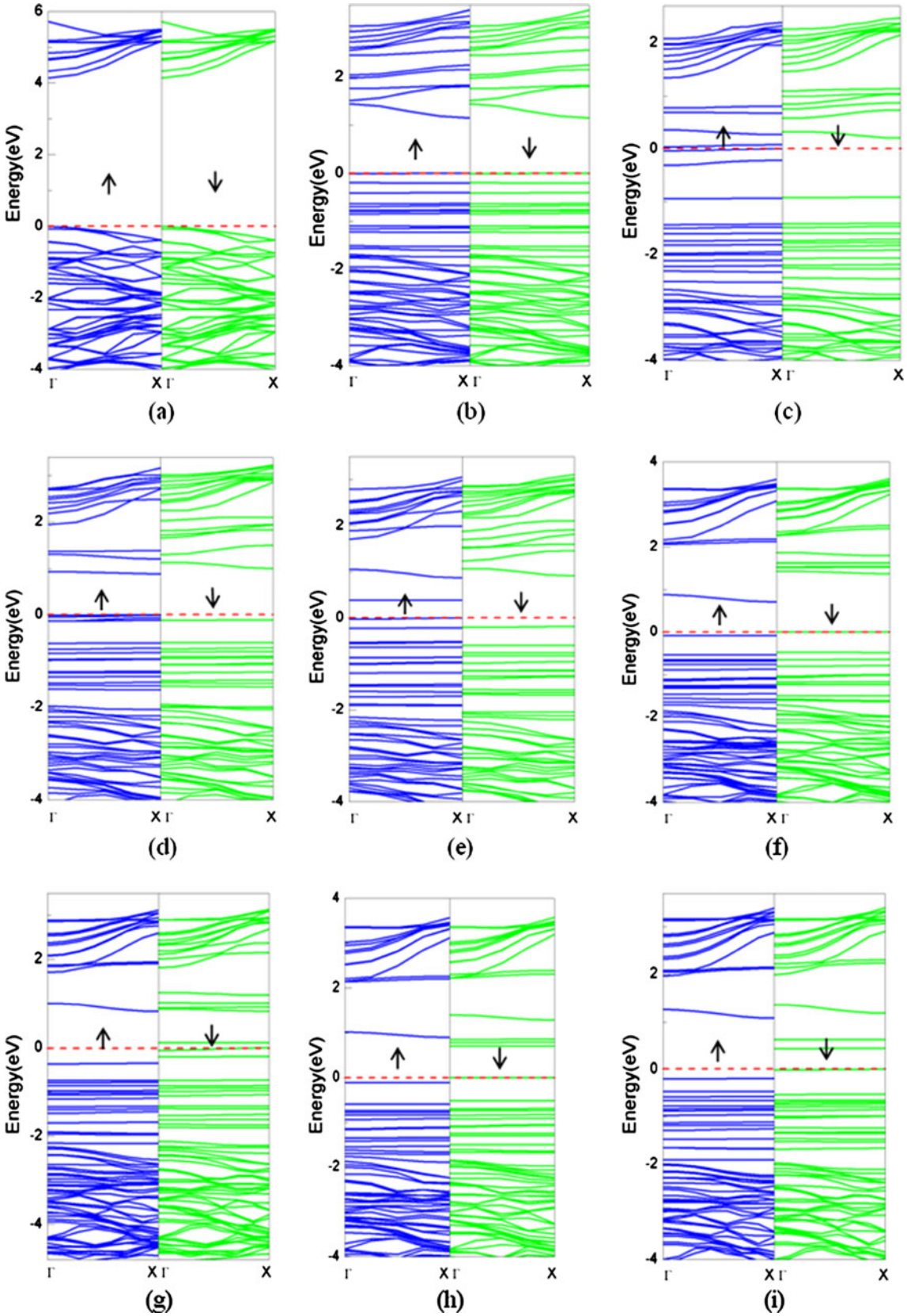

Fig. 4 The band structures of **a** pristine (10, 0) BNNT, and Pd_3M@BNNT, where M is **b** Sc, **c** Ti, **d** V, **e** Cr, **f** Mn, **g** Fe, **h** Co, **i** Ni, **j** Cu, **k** Zn, **l** Pd, **m** Pt, and **n** Au. The plus and minus spin electronic structures are distinguished with "+" and "_". The Fermi level is plotted with the *red dotted line*

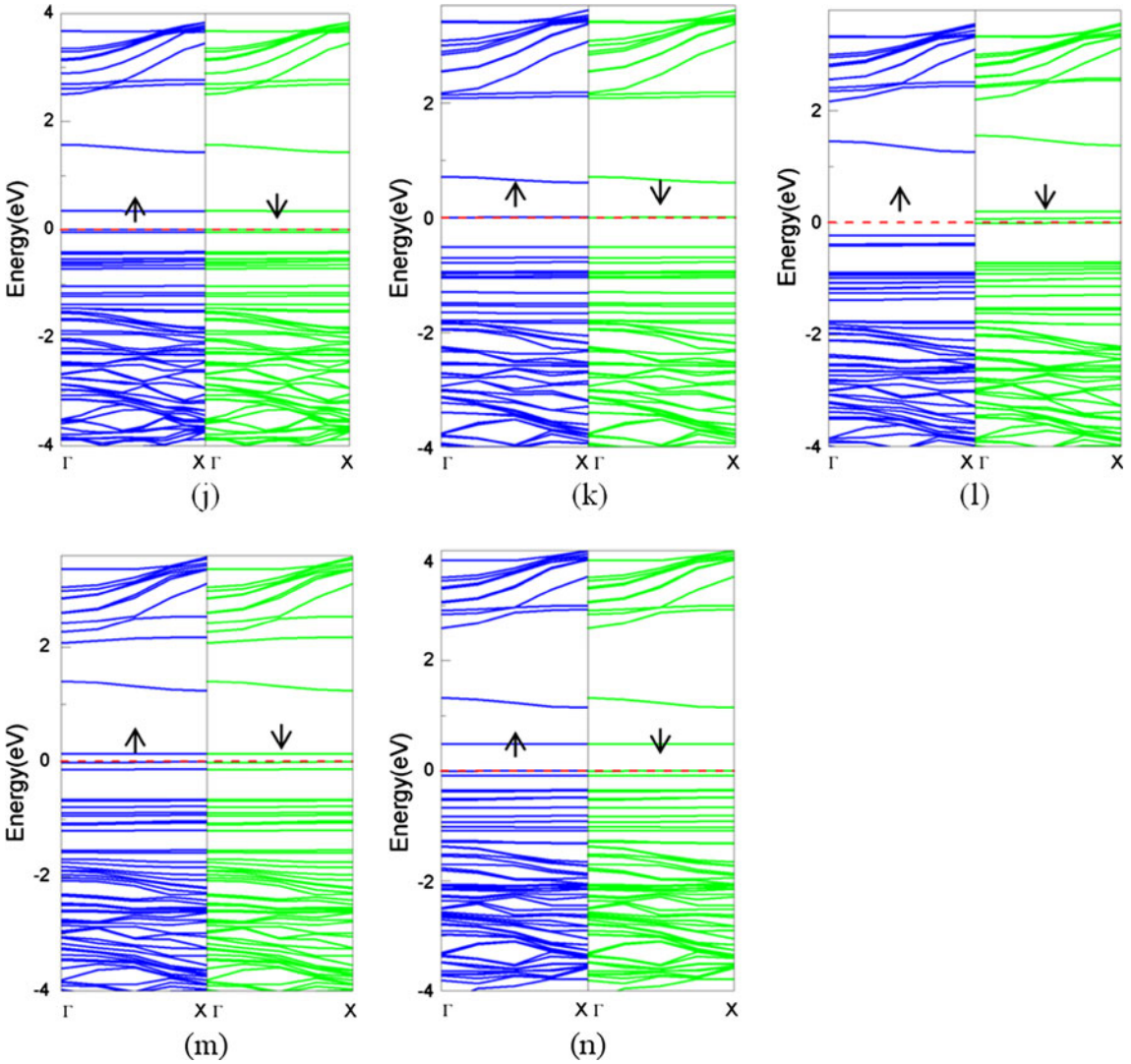

Fig. 4 (continued)

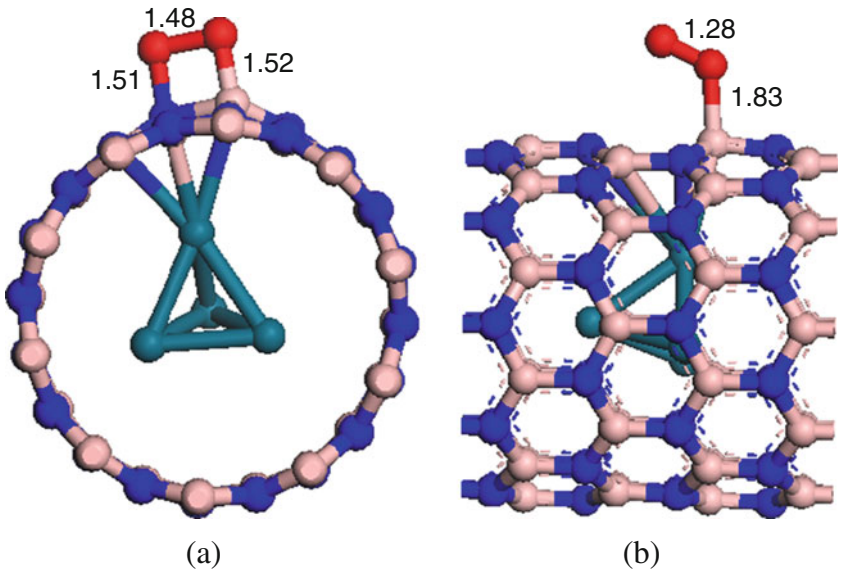

Fig. 5 The optimized stable configurations of a single O_2 molecule adsorbed on Pd_4@BNNT in (**a**) horizontal and (**b**) vertical orientation. The unit of bond length is Å

bond, and hexagon of B_3N_3. The calculated adsorption energies, structural parameters, and charge transfer of O_2 on Pd_3M@BNNTs are shown in Table 2. For the O_2 molecule on pristine BNNT, we find that this kind of adsorption is considerably weaker with E_{ads} of −0.14 eV. The distance between BNNT and the O_2 molecule is 3.12 Å.

In contrast, for Pd_4@BNNT, the O_2 molecule can be stably adsorbed on BNNT. The lowest energy configuration is that O_2 molecule prefers to adsorb in horizontal orientation, as shown in Fig. 5a. For this configuration, the O-O bond is elongated up to 1.48 Å (peroxo type [61]), which is larger than in its free form (1.22 Å). Meanwhile, the O_2 molecule binds with the axial B-N bond with B-O and N-O bond lengths of 1.52 and 1.51 Å, respectively. The energy released during this process is estimated to be 2.36 eV and about 0.22 electrons are transferred from Pd_4@BNNT to O_2 molecule. As shown in Fig. 5b, a meta-stable configuration is also obtained for O_2 adsorption on Pd_4@BNNT, where the O_2 molecule adsorbs on one of B atom of BNNT in elbow shaped orientation. The calculated adsorption energy for this configuration is −0.84 eV. The O-O and O-B bond lengths are 1.28 and 1.83 Å, respectively.

In Table 2, we present the results of O_2 interactions with other Pd_3M@BNNT materials. The results suggest that the binding strength of O_2 molecule with these encapsulated BNNTs is much stronger than that with pristine BNNT in various ways. Moreover, the adsorption energy of O_2 molecule on Pd_3Sc@BNNT is the largest (E_{ads}= −2.09 eV), suggesting a strong chemisorption. Similarly, the encapsulation of Pd_3Ti, Pd_3V, Pd_3Cr, and Pd_3Fe also renders BNNT high chemical reactivity toward O_2 with large adsorption energies of −1.62, −1.18, −0.83, −0.68 eV, respectively. Especially, the O-O bonds of adsorbed O_2 molecules on the above BNNT-based composites are elongated to ~1.33 Å. This fact indicates that the filled BNNTs with Pd_3Sc, Pd_3Ti, Pd_3V, Pd_3Cr, and Pd_3Fe clusters have potential for developing oxidative catalysis. For other Pd_3M@BNNTs (*M*=Mn, Co, Ni, Cu, Zn, Pt, and Au), however, we find that the chemical reactivity of BNNT toward O_2 molecule (E_{ads}=−0.27, −0.27, −0.38, −0.22, −0.27, −0.22, and −0.23 eV, respectively) is slightly stronger than the pristine one (E_{ads}=−0.14 eV). This can be testified by the large distance between BNNT and adsorbates as shown in Table 2. Due to the weak interaction, it is expected that the seven Pd_3M@BNNTs (*M*=Mn, Co, Ni, Cu, Zn, Pt, and Au) are unsuitable for oxidative catalysis. On the basis of the above results, it is found that the binding strength of O_2 with Pd_3M@BNNTs seems to be unrelated with the magnetic momentums of these nanocomposites.

Table 2 The calculated adsorption energy (E_{ads}, eV)[a] of the O_2 molecule on Pd_3M@BNNT, charge transfer from Pd_3M@BNNT to O_2 molecule (*Q*, e), optimized O-O ($d_{O\text{-}O}$), and B-O distances ($d_{B\text{-}O}$, Å). The O-O bond length in the free O_2 molecule is calculated to be 1.22 Å

M	E_{ads},	*Q*	$d_{B\text{-}O}$	$d_{O\text{-}O}$
pure BNNT	−0.14	−0.01	3.12	1.23
Sc	−2.09	−0.27	1.50	1.35
Ti	−1.62	−0.27	1.51	1.35
V	−1.18	−0.26	1.50	1.35
Cr	−0.83	−0.23	1.56	1.33
Mn	−0.27	−0.13	3.12	1.24
Fe	−0.68	−0.22	1.56	1.33
Co	−0.27	−0.13	2.87	1.24
Ni	−0.38	−0.16	2.83	1.25
Cu	−0.22	−0.11	3.08	1.24
Pd	−2.36	−0.22	1.52	1.48
Zn	−0.27	−0.13	3.03	1.24
Pt	−0.22	−0.12	2.92	1.24
Au	−0.23	−0.11	3.13	1.24

[a] The adsorption energy is defined as: $E_{ads}=E_{total}(O_2+Pd_3M@BNNT)-E_{total}(Pd_3M@BNNT)-E_{total}(O_2)$, where E_{total} is the total energy of the system in the bracket

Conclusions

In summary, we have carried out density functional theory study to calculate the equilibrium structures and energetics of different small Pd_3M clusters (*M*=Sc, Ti, V, Cr, Mn, Fe, Co, Ni, Cu, Zn, Pd, Pt, and Au) encapsulated in (10, 0) BNNT. In particular, the effects of the Pd_3M-encapsulation on the electronic and magnetic properties are mainly addressed. The results indicate that these considered Pd_3M clusters can be stably filled in (10, 0) BNNT. The band structures of Pd_3M@BNNTs show that some new impurity bands are introduced to the large band gap of the pristine BNNT, rendering it to exhibit semiconducting nature, whose band gaps are less than 1.0 eV. Moreover, the encapsulation of the Pd_3M clusters can give rise to a variety of net magnetic moments, ranging from 5.08 μ_B to 0. Finally, by studying the interaction of BNNT and O_2 molecules, we find that the encapsulated BNNTs by Pd_3M cluster (*M*=Sc, Ti, V, Cr, Fe, and Pd) exhibit a much higher chemical reactivity than the pristine one. The elongation of the O–O bonds of adsorbed O_2 molecules indicates that several Pd_3M@BNNTs can also be used for further industrial catalytic applications. Though the current DMol3 based DFT-GGA calculations are not very accurate in terms of the absolute magnitude of band gap, we expect that our qualitative results on the effects of Pd_3M encapsulation on the electronic properties of the BNNT remain robust with respect to more accurate calculations.

Acknowledgments This work is supported by the National Nature Science Foundation of China (No. 21203048) and University Key Teacher Foundation of Heilongjiang Provincial Education Department (No. 1252G030).

References

1. Iijima S (1991) Nature 354:56–58
2. Rubio A, Corkill JL, Cohen ML (1994) Phys Rev B 49:5081–5084
3. Golberg D, Bando Y, Tang CC, Zhi CY (2007) Adv Mater 19:2413–2432
4. Zhi CY, Bando Y, Tang CC, Golberg D (2010) Mater Sci Eng R Rep 70:92–111
5. Hernandez E, Goze C, Bernier P, Rubio A (1998) Phys Rev Lett 80:4502–4505
6. Suryavanshi AP, Yu M, Wen J, Tang CC, Bando Y (2004) Appl Phys Lett 84:2527–2529
7. Han WQ, Bando Y, Kurashima K, Sato T (1998) Appl Phy Lett 73:3085–3087
8. Xie SY, Wang W, Fernando KAS, Wang X, Lin Y, Sun YP (2005) Chem Comm 29:3670–3672
9. Zhi CY, Bando Y, Tang CC, Honda S, Sato K, Kuwahara H, Golberg D (2005) Ange Chem Inter Ed 44:7932–7935
10. Zhi CY, Bando Y, Tang CC, Xie R, Sekiguchi T, Golberg D (2005) J Am Chem Soc 127:15996–15997
11. Zhi CY, Bando Y, Tang CC, Golberg D (2006) Phys Rev B 74:153413
12. Zhi CY, Bando Y, Tang CC, Huang Q, Golberg D (2008) J Mater Chem 18:3900–3908
13. Wu XJ, Yang JL, Hou JG, Zhu QS (2004) J Chem Phys 121:8481–8485
14. Han SS, Lee SH, Kang JK, Lee HM (2005) Phys Rev B 72:113402
15. Zhou Z, Zhao JJ, Chen ZF, Gao XP, Yan TY, Wen B, Schleyer PV (2006) J Phys Chem B 110:13363–13369
16. Li F, Zhu ZH, Zhao MW, Xia YY (2008) J Phys Chem C 112:16231–16237
17. Xiang HJ, Yang JL, Hou JG, Zhu QS (2005) Appl Phys Lett 87:243113
18. Zhou Z, Zhao JJ, Chen ZF, Schleyer PV (2006) J Phys Chem B 110:25678–25685
19. Lai L, Song W, Lu J, Gao ZX, Nagase S, Ni M, Mei WN, Liu JJ, Yu DP, Ye HQ (2006) J Phys Chem B 110:14092–14097
20. Li F, Zhu ZH, Yao XD, Lu GQ, Zhao MW, Xia YY, Chen Y (2008) Appl Phys Lett 92:102515
21. Zhang J, Loh KP, Yang WS, Wu P (2005) Appl Phys Lett 87:243105
22. Zhang ZH, Guo WL (2009) J Am Chem Soc 131:6874–6879
23. Wu XJ, Zeng XC (2006) J Chem Phys 125:044711
24. Wu XJ, An W, Zeng XC (2006) J Am Chem Soc 128:12001–12006
25. Li YF, Zhou Z, Zhao JJ (2007) J Chem Phys 127:184705
26. Su MD (2005) J Phys Chem B 109:21647–21657
27. Li YF, Zhou Z, Zhao JJ (2008) Nanotech 19:015202–015208
28. Cao FL, Ren W, Xu XY, Li YM, Zhao CY (2009) Phys Chem Chem Phys 11:6256–6262
29. Li J, Zhou G, Liu HT, Duan WH (2006) Chem Phys Lett 426:148–154
30. Li J, Zhou G, Chen Y, Gu BL, Duan WH (2009) J Am Chem Soc 131:1796–1801
31. Gou GY, Pan BC, Shi L (2010) ACS Nano 4:1313–1320
32. Zhao JX, Ding YH (2010) Diam Relat Mater 19:1073–1077
33. Mickelson W, Aloni S, Han WQ, Cumings J, Zettl A (2003) Science 300:467–469
34. Golberg D, Bando Y, Kurashima K, Sato T (2001) J Nanosci Nanotech 1:49–54
35. Li YB, Dorozhkin PS, Bando Y, Golberg D (2005) Adv Mater 17:545–549
36. Golberg D, Bando Y, Fushimi K, Mitome M, Bourgeois L, Tang CC (2003) J Phys Chem B 107:8726–8729
37. Xiang HJ, Yang JL, Hou JG, Zhu QS (2005) New J Phys 7:39
38. Zhang JM, Wang SF, Du XJ, Xu KW, Ji V (2009) J Phys Chem C 113:17745–7750
39. Wang SF, Zhang JM, Xu KW (2010) Phys B 405:1035
40. Xie Y, Zhang JM (2012) J Phys Chem Solids 73:530–534
41. Chen Q, Li F, Dong X, Liu X, Zhao M, Zhou Y, Ma S, Li S (2010) Euro Lett 90:47003
42. Alencar A, Azevedo S, Machado M (2011) Appl Phys A 102:583–591
43. Zhou Z, Zhao JJ, Chen ZF, Gao XP, Lu JP, Von P, Schleyer R, Yang CK (2006) J Phys Chem B 110:2529–2532
44. Ghosh S, Nigam S, Das GP, Majumdar C (2010) J Chem Phys 132:164704
45. Delley B (1990) J Chem Phy 92:508–517
46. Delley B (2000) J Chem Phys 113:7756–7764
47. Perdew JP, Burke K, Ernzerhof M (1996) Phys Rev B 77:3865–3868
48. Perdew JP, Wang Y (1992) Phys Rev B 45:13244–13249
49. Cobian M, Iniguez J (2008) J Phys Condens Matter 20:285212
50. Ataca C, Aktürk E, Ciraci S, Ustunel H (2008) Appl Phys Lett 93:043123
51. Andres PL, Ramírez R, Vergés JA (2008) Phys Rev B 77:045403
52. Cabria I, López MJ, Alonso JA (2005) J Chem Phys 123:204721
53. Okamoto Y, Miyamoto Y (2001) J Phys Chem B 105:3470–3474
54. Wu XJ, Gao Y, Zeng XC (2008) J Phys Chem C 112:8458–8463
55. Zhao JJ, Liu JP (2001) Appl Rev Lett 82:3746–3748
56. Lin ZY, Wang YB (2003) J Am Chem Soc 125:6072–6073
57. Lu J, Lai L, Luo GF, Zhou J, Qin R, Wang D, Wang L, Mei WN, Li GP, Gao ZX, Nagase S, Maeda Y, Akasaka T, Yu DP (2007) Small 3:1566–1576
58. Improta R, Barone V, Kudin KN, Scuseria GE (2001) J Am Chem Soc 123:3311–3322
59. Hirshfeld FL (1977) Theo Chim Acta 44:129–138
60. Monkhorst HJ, Pack JD (1976) Phys Rev B 13:5188–5192
61. Gutsev GL, Rao BK, Jena P (2000) J Phys Chem A 104:11961–11971